Fault zone properties affecting the rupture evolution of the 2009 (M_w 6.1) L'Aquila earthquake (central Italy): Insights from seismic tomography

R. Di Stefano,[1] C. Chiarabba,[1] L. Chiaraluce,[1] M. Cocco,[1] P. De Gori,[1] D. Piccinini,[1] and L. Valoroso[1]

Received 4 March 2011; revised 20 April 2011; accepted 20 April 2011; published 28 May 2011.

[1] We have inverted P- and S-wave travel times from seismograms recorded by a dense local network to infer the velocity structure in the crustal volume where the April 6th 2009 main shock nucleated. The goal is to image local variations of P-wave velocity and Poisson ratio along the main shock fault zone for interpreting the complexity of the rupture history. The initial stages of the mainshock rupture are characterized by an emergent phase (EP) followed by an impulsive phase (IP) 0.87 s later. The EP phase is located in a very high V_P and relatively low Poisson ratio (ν) region. The IP phase marks the beginning of the large moment release and is located outside the low ν volume. The comparison between the spatial variations of V_P and Poisson ratio within the main shock nucleation volume inferred in this study with the rupture history imaged by inverting geophysical data allows us to interpret the delayed along-strike propagation in terms of heterogeneity of lithology and material properties. **Citation:** Di Stefano, R., C. Chiarabba, L. Chiaraluce, M. Cocco, P. De Gori, D. Piccinini, and L. Valoroso (2011), Fault zone properties affecting the rupture evolution of the 2009 (M_w 6.1) L'Aquila earthquake (central Italy): Insights from seismic tomography, *Geophys. Res. Lett.*, *38*, L10310, doi:10.1029/2011GL047365.

1. Introduction

[2] The M_W 6.1 April 6th (01:32 UTC) 2009 L'Aquila earthquake ruptured a ~16 km long, ~50° SW-dipping normal fault located in the central Apennines [*Chiarabba et al.*, 2009; *Scognamiglio et al.*, 2010; *Chiaraluce et al.*, 2011]. Several recent studies have emphasized the complexity of the rupture process including both the earthquake nucleation and the subsequent coseismic rupture propagation [*Ellsworth and Chiaraluce*, 2009]. The source models imaged by inverting strong motion waveforms, GPS displacements and DinSar data [*Anzidei et al.*, 2009; *Atzori et al.*, 2009; *Cirella et al.*, 2009; *Pino and Di Luccio*, 2009; *Cheloni et al.*, 2010] reveal a heterogeneous slip distribution on the fault plane characterized by two main slip patches, situated up-dip from the hypocenter (located at a depth of 8.6 km, see Table S1 in Text S1 of the auxiliary material) and 4 km south-eastward along the strike, respectively.[1] Despite the relatively moderate magnitude of the event, rupture directivity characterizes the observed ground motions [*Cirella et al.*, 2009; *Pino and Di Luccio*, 2009] and relatively high acceleration amplitudes were recorded at strong motion receivers around the L'Aquila city [*Ameri et al.*, 2009; *Çelebi et al.*, 2010], located on the fault hanging-wall above the hypocenter.

[3] Soon after the main shock a temporary network consisting of 40 digital seismic stations was installed by a team composed by researchers of the Istituto Nazionale di Geofisica e Vulcanologia (INGV) and the Laboratoire de Géophysique Interne et Tectonophysique (LGIT) of Grenoble [*Chiaraluce et al.*, 2011]. The seismograms recorded by this temporary network have been integrated with those recorded by the closest 17 stations of the permanent national INGV network. The network geometry and aftershocks catalogue are discussed in the auxiliary material.

[4] The goal of this paper is to image the velocity structure in the source volume with the objective of investigating the role played by the material properties during coseismic faulting, which likely control the observed complex rupture history of the main shock. V_P and Poisson ratio models are good tools to infer fault frictional properties [*Lees and Nicholson*, 1993; *Thurber et al.*, 1995; *Zhao et al.*, 1996; *Eberhart-Phillips and Michael*, 1998; *Zhao and Negishi*, 1998]. High-resolution crustal velocity models for the study area can be computed thanks to the availability of a huge quantity of well-recorded earthquakes and high quality of P- and S-wave arrival times [*Aldersons et al.*, 2009; *Valoroso and L'Aquila 2009 Mobile Network Working Group*, 2009]. Figure 1 shows the aftershock distribution relocated with the 3D velocity model computed in this study. Figure 1 clearly shows that two main distinct fault segments were activated during the 2009 L'Aquila sequence (near L'Aquila and Campotosto [see *Chiarabba et al.*, 2009]). In this study, we only focus on the main shock fault (see box in Figure 1). A more complete discussion of the whole aftershock sequence and the spatial pattern of seismicity is given by *Chiaraluce et al.* [2011].

2. The Velocity Model

[5] We have extracted a sub-set of aftershocks recorded at the dense network of 57 seismic stations (see Figure S1 of the auxiliary material) during the first 3 months of the sequence (April-June, 2009). Earthquakes are first located

[1]Istituto Nazionale di Geofisica e Vulcanologia, Rome, Italy.

0094-8276/11/2011GL047365

[1]Auxiliary materials are available in the HTML. doi:10.1029/2011GL047365.

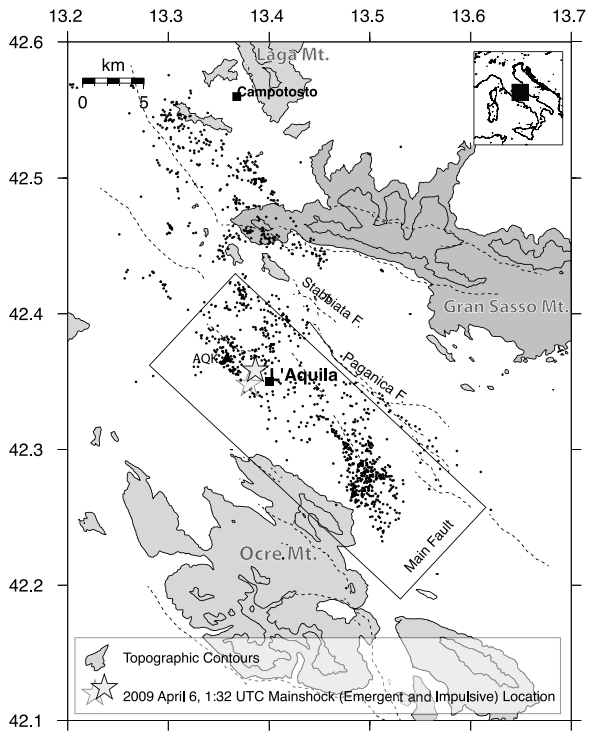

Figure 1. Map of seismicity located with the 3D velocity model inferred in this study. The NW-SE oriented rectangle displays the surface projection of the main shock fault plane. Black dots are the aftershocks' locations. Dashed lines are the mapped faults while the black solid line is the mapped surface breakage of the Paganica Fault caused by the April 6th 2009 mainshock. The black triangle is the strong motion station AQK (see Figure S3 of the auxiliary material).

with the 1D velocity model proposed by *Chiarabba et al.* [2009]. The selected dataset consists of 1276 events having location errors less than 1 km and azimuthal gap <180°. P-wave and S-P arrival times are then inverted using the Simulps14 algorithm [*Haslinger*, 1998].

[6] The velocity model is parameterized by linearly interpolating between values assigned and modified at a 3D grid of nodes, with node spacing of 5 km horizontally and 2 km vertically. This spacing well optimizes image fidelity and model resolution, for the given distribution of earthquakes and stations. We use 44445 P- and 14801 S-wave arrivals to solve for 2655 velocity and 5104 hypocentral parameters. The final model rms is 0.08, corresponding to a data weighted variance improvement of 65%, achieved after 4 iterative steps (see the auxiliary material for additional details). Model resolution is verified analyzing the entire resolution matrix, i.e., via the spread function, averaging vectors and diagonal elements [*Menke*, 1989]. The resolution of the V_P and V_P/V_S model is very high (see Figure S2 of the auxiliary material), and therefore the retrieved velocity values in the volume around the L'Aquila main shock fault plane are reliable.

[7] Figure 2a shows V_P and Poisson ratio (computed from V_P/V_S; see auxiliary material) maps imaged at 4 km, 6 km, and 8 km depth where most of the aftershocks are located. Contour lines of the spread function having a value of 2 are displayed in each panel (black solid line); this threshold identifies the well-resolved parameters, according to the inspection of averaging vectors [see *Toomey and Foulger*, 1989; *Reyners et al.*, 1999]. Thus the contour line encloses the well-resolved volume for both models.

[8] Relevant high V_P and low ν anomalies (see auxiliary material for details on the reference ν value) characterize the crustal structure around the fault zone at 6 and 8 km depth. P-wave velocities are higher than 6.6 km/s between 5 and 7 km of depth (Figure 2). These values are higher than those observed in laboratory experiments by *Trippetta et al.* [2010], at high confining pressure (depth > 4 km), for limestone and Triassic Evaporites (alternating sulphates and dolostones) commonly characterizing the lower portion of the upper crust in this sector of the Apennines. Such high V_P anomalies, continuing toward the SW between 7 and 9 km, can be ascribed to a mafic basement, consistently with recent results by *Chiarabba et al.* [2010].

[9] A vertical cross section perpendicular to the main shock fault plane (Figure 2b) shows that the normal fault and seismicity are located in a complex velocity structure, made of a pile of Meso-Cenozoic sedimentary cover and underlying high V_P basement (see dashed line in Figure 2b), obducted during the Mio-Pliocene compressional event [*Bianchi et al.*, 2010]. Aftershocks (black dots) delineate a nearly 50° SW-dipping fault, with a slight flattening at the upper tip. The upward continuation of the aftershocks coincides with the mapped surface trace of the San Demetrio-Paganica and Stabbiata faults and with the mapped ruptures observed along the Paganica fault related to the L'Aquila mainshock [*EMERGEO Working Group*, 2009; *Boncio et al.*, 2010]. The extreme heterogeneity in the upper crust, resulting from the previous compressional tectonic phase, may be explained with the presence of a laterally irregular pile of mafic basement and sedimentary cover (very high V_P and relatively low ν values) stacked during the Apennines belt formation. In this interpretation, the main-shock nucleated within the high V_P basement.

3. The Mainshock Rupture Onset

[10] The analysis of the closest strong motion accelerograms reveals that the initial stages of the main shock rupture are rather complex. Indeed, ground motion time histories show an initial emergent P-wave signal (hereinafter EP) followed by an impulsive onset (IP) (see Figure S3). These two phases are visible at permanent seismic stations located within 80 kilometers of distance both on digital and analogic recording stations. This latter circumstance allows us to exclude artifacts due to finite impulse response (FIR) [*Scherbaum and Bouin*, 1997]. We have used 33 and 18 high quality arrival times of EP and IP phases, respectively, in order to locate the points on the fault where they are radiated. The inferred 3D velocity model allows constraining high quality locations for both phases having formal errors around 0.1 km in latitude, longitude and depth. Hypocentral coordinates and errors are listed in Table S1 (see auxiliary material). These results show that the source of the IP phase is located nearly 2 km up-dip from that of the EP phase (see stars in Figure 2). The difference between their origin times is 0.87 s. This is consistent with the retrieved up-dip initial rupture propagation [*Cirella et al.*, 2009; *Pino and Di Luccio*, 2009] as well as with the complex rupture onset [*Ellsworth and Beroza*, 1995; *Beroza and*

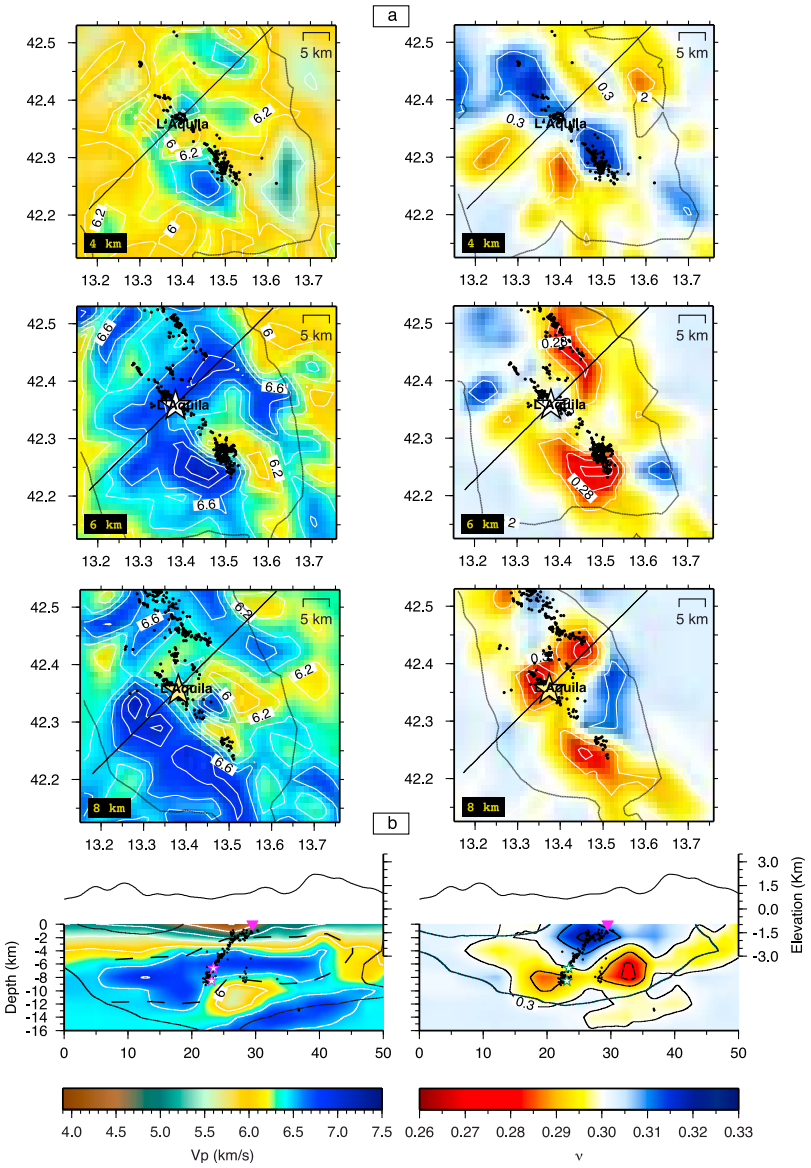

Figure 2. (a) Map view of V_P and ν (Poisson ratio) values imaged at 4 km, 6 km, and 8 km depth. The black solid line represents the contour line of the spread function (spf) = 2, which encloses the well-resolved volumes. Earthquakes occurring within ±1 km from each layer are plotted. The yellow and white stars are the locations of the EP and IP phases of the main-shock respectively. The straight black line is the trace of the vertical section (see Figure 2b). (b) Vertical section across the fault. The black solid lines indicate the well-resolved volume. Aftershocks occurring within ±1 km from the section are shown.

Ellsworth, 1996] inferred by analyzing high frequency ground motion waveforms [*Ellsworth and Chiaraluce*, 2009; *Michelini et al.*, 2009].

4. Discussion

[11] Spatial heterogeneity of strength or frictional properties along active faults has been widely evoked to explain complex ruptures of large earthquakes [e.g., *Zhao et al.*, 1996; *Boatwright and Cocco*, 1996]. Body wave velocities and Poisson ratio are a rationale proxy to image the physical properties of rocks [*Zhao et al.*, 1996], being related to their composition, crack density, fluids and temperature. Lateral variations of material properties along faults are widely documented worldwide, and changes of ν in the source region of large magnitude earthquakes are often related to fluids [*Zhao and Negishi*, 1998; *Wang and Zhao*, 2006].

[12] The 3-D crustal velocity model inferred in this study allows us to discuss some features of relevance for the interpretation of the main shock initiation and the subsequent rupture propagation. Figure 3 shows the V_P and Poisson ratio (ν) models imaged on a NW-SE and 50° SW-dipping section containing the main shock fault plane. The most significant feature is that the EP hypocenter is located within a high V_P and relatively low ν volume (<0.3), while the IP location lies up-dip in a transition area between low and average ν values (~0.3). Poisson ratio values as low as 0.28 are in fact equal or less than those measured in labo-

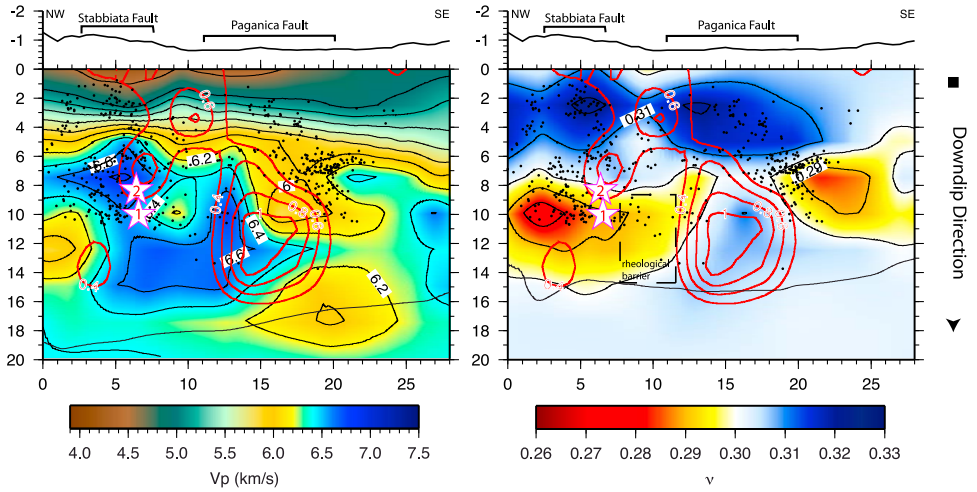

Figure 3. V_P and ν values imaged along the 50° SW-dipping and N133° striking main shock fault plane. The black solid lines indicate the spf = 2 (see Figure 2). The co-seismic slip by *Cirella et al.* [2009] is plotted (red solid contouring). The EP (1) and IP (2) locations (open stars), and the aftershocks 3D locations (black dots) are also plotted. The dashed box identifies the position of the speculated rheological barrier which likely delayed the along strike rupture propagation.

ratory for dry sulphates and dolostones, independent from confining pressure [*Trippetta et al.*, 2010]. Moreover, we observe that the main slip patches imaged by inverting strong motion and GPS data [*Cirella et al.*, 2009] are located in areas where Poisson ratio is ≅0.3, which is the reference mean value for the target region based on the average V_P/V_S of 1.88 (see auxiliary material).

[13] According to recent studies imaging the rupture history of the L'Aquila main shock [*Cirella et al.*, 2009; *Ellsworth and Chiaraluce*, 2009; *Piatanesi et al.*, 2009], we know that the rupture initially propagated up-dip from the hypocenter and only after nearly 2 s it started to propagate along strike. Therefore, there is a delay in rupturing the main slip patch at depth. It is worth noting that the transition between low ν in the nucleation zone and higher ν in the high slip patch nearly coincides with the zone where along strike rupture has been initially impeded and delayed [*Cirella et al.*, 2009]. These results allow us to interpret the inferred spatial variations of crustal properties in terms of features affecting dynamic rupture propagation.

[14] In the upper portion of the fault, V_P values range between 4.5 km/s and 5.7 km/s, which correspond to the shallow sedimentary cover extending 6 km downdip (Figure 3). In this region high ν values, corresponding to V_P/V_S higher than 1.9, characterize areas of small co-seismic slip.

[15] *Lucente et al.* [2010] report evidence for temporal variability of V_P/V_S ratio before the L'Aquila main shock by modeling the foreshock data. In particular, they suggest that the March 30th 2009 foreshock promoted a rapid increase of the V_P/V_S ratio in the hangingwall volume that lasted until the L'Aquila main shock. This might imply that the rupture nucleated in a fluid infiltrated volume. The 3D crustal model presented in this study is obtained by inverting aftershocks travel times; therefore, it provides an image of velocity anomalies present in the studied volume after and maybe during the co-seismic rupture. After the nucleation, the rupture initially propagated within a low ν volume and after 0.87 seconds accelerated and propagated nearly unidirectional up-dip for few seconds, within areas of normal ν and where V_P ranges between 5.5–6.6 km/s. The low ν values around the hypocenter (EP) might imply that, if present during nucleation, fluids escaped from the hypocentral area. This is also consistent with the complex spatial pattern of foreshocks hypocenters, showing the activation of secondary fault planes different from the main shock rupture plane [*Chiaraluce et al.*, 2011].

[16] Our results support the idea that strong spatial variations of material properties along faults can control the rupture propagation during moderate-to-large magnitude earthquakes.

5. Conclusions

[17] The complexity of the tectonic setting and the contemporary availability of high quality seismological data make the L'Aquila earthquake a good example to investigate the relation between heterogeneity of material properties and co-seismic rupture history for normal faulting earthquakes. Our results demonstrate that rupture initially propagated in an area characterized by relatively low values of Poisson ratio ($\nu < 0.3$) and characterized by a small moment release (EP phase). This initial rupture process lasted nearly 0.87 s (Table S1). Considering that the locations of the EP and IP phases are separated by nearly 2 km along the fault plane, the rupture propagated during this first ~0.9 s at a relatively high speed, which allows us to exclude a slow initial process (propagation velocity ranges between 2.2 and 3.4 km/s) or demand for a dynamic triggering. After this initial stage, the rupture propagated up-dip within the region of higher Poisson Ratio. The beginning of this stage is marked by the onset of the IP phase.

[18] The main slip patch located at depth southeastward along the strike direction, whose failure was delayed, lies in an area characterized by values of $\nu \geq 0.3$. Therefore, we conclude that the geological conditions in the area separating the lower and higher patches of Poisson ratio have impeded the immediate rupture propagation along strike delaying the onset of co-seismic slip. This allows us to

speculate that a rheological barrier delayed the rupture propagation along the strike direction and the failure of the deep asperity.

[19] **Acknowledgments.** Our paper was strongly improved during the revision process thanks to the reviewers' comments. For this reason we would like to sincerely thank Bill Ellsworth, Junichi Nakajima, and the anonymous third reviewer.

[20] The Editor thanks William Ellsworth and an anonymous reviewer for their assistance in evaluating this paper.

References

Aldersons, F., L. Chiaraluce, R. Di Stefano, D. Piccinini, and L. Valoroso (2009), Automatic detection, and P- and S-wave picking algorithm: An application to the 2009 L'Aquila (central Italy) earthquake sequence, *Eos Trans. AGU*, *90*(52), Fall Meet. Suppl., Abstract U23B-0045.

Ameri, G., et al. (2009), The 6 April 2009 Mw 6.3 L'Aquila (central Italy) earthquake, strong motion observations, *Seismol. Res. Lett.*, *80*, 951–966, doi:10.1785/gssrl.80.6.951.

Anzidei, M., et al. (2009), Coseismic deformation of the destructive April 6, 2009 L'Aquila earthquake (central Italy) from GPS data, *Geophys. Res. Lett.*, *36*, L17307, doi:10.1029/2009GL039145.

Atzori, S., I. Hunstad, M. Chini, S. Salvi, C. Tolomei, C. Bignami, S. Stramondo, E. Trasatti, A. Antonioli, and E. Boschi (2009), Finite fault inversion of DInSAR coseismic displacement of the 2009 L'Aquila earthquake (central Italy), *Geophys. Res. Lett.*, *36*, L15305, doi:10.1029/2009GL039293.

Beroza, G. C., and W. L. Ellsworth (1996), Properties of the seismic nucleation phase, *Tectonophysics*, *261*(1–3), 209–227, doi:10.1016/0040-1951(96)00067-4.

Bianchi, I., C. Chiarabba, and N. Piana Agostinetti (2010), Control of the 2009 L'Aquila earthquake, central Italy, by a high-velocity structure: A receiver function study, *J. Geophys. Res.*, *115*, B12326, doi:10.1029/2009JB007087.

Boatwright, J., and M. Cocco (1996), Frictional constraints on crustal faulting, *J. Geophys. Res.*, *101*(B6), 13,895–13,909, doi:10.1029/96JB00405.

Boncio, P., A. Pizzi, F. Brozzetti, G. Pomposo, G. Lavecchia, D. Di Naccio, and F. Ferrarini (2010), Coseismic ground deformation of the 6 April 2009 L'Aquila earthquake (central Italy, M_W 6.3), *Geophys. Res. Lett.*, *37*, L06308, doi:10.1029/2010GL042807.

Çelebi, M., et al. (2010), Recorded motions of the 6 April 2009 Mw 6.3 L'Aquila, Italy, 651 earthquake and implications for building structural damage: Overview, *Earthquake Spectra*, *26*, 651–684, doi:10.1193/1.3450317.

Cheloni, D., et al. (2010), Coseismic and initial post-seismic slip of the 2009 Mw 6.3 L'Aquila earthquake, Italy, from GPS measurements, *Geophys. J. Int.*, *181*, 1539–1546, doi:10.1111/j.1365-246X.2010.04584.x.

Chiarabba, C., et al. (2009), The 2009 L'Aquila (central Italy) M_W 6.3 earthquake: Main shock and aftershocks, *Geophys. Res. Lett.*, *36*, L18308, doi:10.1029/2009GL039627.

Chiarabba, C., S. Bagh, I. Bianchi, P. De Gori, and M. Barchi (2010), Deep structural heterogeneities and the tectonic evolution of the Abruzzi region (Central Apennines, Italy) revealed by microseismicity, seismic tomography, and teleseismic receiver functions, *Earth Planet. Sci. Lett.*, *295*(3–4), 462–476, doi:10.1016/j.epsl.2010.04.028.

Chiaraluce, L., C. Chiarabba, P. De Gori, R. Di Stefano, L. Improta, D. Piccinini, A. Schlagenhauf, P. Traversa, L. Valoroso, and C. Voisin (2011), The April 2009 L'Aquila (central Italy) seismic sequence, *Boll. Geofis. Teor. Appl.*, in press.

Cirella, A., A. Piatanesi, M. Cocco, E. Tinti, L. Scognamiglio, A. Michelini, A. Lomax, and E. Boschi (2009), Rupture history of the 2009 L'Aquila (Italy) earthquake from non-linear joint inversion of strong motion and GPS data, *Geophys. Res. Lett.*, *36*, L19304, doi:10.1029/2009GL039795.

Eberhart-Phillips, D., and A. J. Michael (1998), Seismotectonics of the Loma Prieta, California, region determined from three-dimensional Vp, Vp/Vs and seismicity, *J. Geophys. Res.*, *103*(B9), 21,099–21,120, doi:10.1029/98JB01984.

Ellsworth, W. L., and G. C. Beroza (1995), Seismic evidence for an earthquake nucleation phase, *Science*, *268*(5212), 851–855, doi:10.1126/science.268.5212.851.

Ellsworth, W. L., and L. Chiaraluce (2009), Supershear during nucleation of the 2009 M 6.3 L'Aquila, Italy earthquake, *Eos Trans. AGU*, *90*(52), Fall Meet. Suppl., Abstract U13C-07.

EMERGEO Working Group (2009), Evidence for surface rupture associated with the Mw 6.3 L'Aquila earthquake sequence of April 2009 (central Italy), *Terra Nova*, *22*, 43–51, doi:10.1111/j.1365-3121.2009.00915.x.

Haslinger, F. (1998) Velocity structure, seismicity and seismotectonics of northwestern Greece between the Gulf of Arta and Zakynthos, Ph.D. thesis, Dep. Geophys., ETH, Zurich, Switzerland.

Lees, J. M., and C. Nicholson (1993), Three-dimensional tomography of the 1992 Southern California earthquake sequence: Constraints on dynamic earthquake rupture?, *Geology*, *21*(5), 387–390, doi:10.1130/0091-7613(1993)021<0387:TDTOTS>2.3.CO;2.

Lucente, F. P., P. De Gori, L. Margheriti, D. Piccinini, M. Di Bona, C. Chiarabba, and N. Piana Agostinetti (2010), Temporal variation of seismic velocity and anisotropy before the 2009 M_W 6.3 L'Aquila earthquake, Italy, *Geology*, *38*(11), 1015–1018, doi:10.1130/G31463.1.

Menke, W. (1989), *Geophysical Data Analysis: Discrete Inverse Theory*, Academic, New York.

Michelini, A., L. Faenza, A. Lomax, and M. Cocco (2009), Appraisal of the hypocentral location of the L'Aquila main shock, *Eos Trans. AGU*, *90*(52), Fall Meet. Suppl., Abstract U23A-0027.

Piatanesi, A., A. Cirella, M. Cocco, E. Tinti, L. Scognamiglio, A. Michelini, A. Lomax, and A. Lomax (2009), The rupture history of the 2009 L'Aquila earthquake by non-linear joint inversion of strong motion and GPS data, *Eos Trans. AGU*, *90*(52), Fall Meet. Suppl., Abstract U13C-05.

Pino, N. A., and F. Di Luccio (2009), Source complexity of the 6 April 2009 L'Aquila (central Italy) earthquake and its strongest aftershock revealed by elementary seismological analysis, *Geophys. Res. Lett.*, *36*, L23305, doi:10.1029/2009GL041331.

Reyners, M., D. Eberhart-Phillips, and G. Stuart (1999), A three-dimensional image of shallow subduction: Crustal structure of the Raukumara Peninsula, New Zealand, *Geophys. J. Int.*, *137*, 873–890, doi:10.1046/j.1365-246x.1999.00842.x.

Scherbaum, F., and M.-P. Bouin (1997), FIR filter effects and nucleation phases, *Geophys. J. Int.*, *130*, 661–668, doi:10.1111/j.1365-246X.1997.tb01860.x.

Scognamiglio, L., E. Tinti, A. Michelini, D. S. Dreger, A. Cirella, M. Cocco, S. Mazza, and A. Piatanesi (2010), Fast determination of moment tensors and rupture history: What has been learned from the 6 April 2009 L'Aquila earthquake sequence, *Seismol. Res. Lett.*, *81*(6), 892–906, doi:10.1785/gssrl.81.6.892.

Thurber, C. H., S. R. Atre, and D. Eberhart-Phillips (1995), Three-dimensional Vp and Vp/Vs structure at Loma Prieta, California, from local earthquake tomography, *Geophys. Res. Lett.*, *22*(22), 3079–3082, doi:10.1029/95GL03077.

Toomey, D. R., and G. R. Foulger (1989), Tomographic inversion of local earthquake data from the Hengill-Grensdalur central volcano complex, Iceland, *J. Geophys. Res.*, *94*(B12), 17,497–17,510, doi:10.1029/JB094iB12p17497.

Trippetta, F., C. Collettini, S. Vinciguerra, and P. G. Meredith (2010), Laboratory measurements of the physical properties of Triassic Evaporites from central Italy and correlation with geophysical data, *Tectonophysics*, *492*, 121–132, doi:10.1016/j.tecto.2010.06.001.

Valoroso, L., and L'Aquila 2009 Mobile Network Working Group (2009), The 2009 L'Aquila seismic sequence (central Italy): Fault system geometry and kinematics, *Eos Trans. AGU*, *90*(52), Fall Meet. Suppl., Abstract U12A-04.

Wang, Z., and D. Zhao (2006), Seismic images of the source area of the 2004 Mid-Niigata prefecture earthquake in northeast Japan, *Earth Planet. Sci. Lett.*, *244*, 16–31, doi:10.1016/j.epsl.2006.02.015.

Zhao, D., and H. Negishi (1998), The 1995 Kobe earthquake: Seismic image of the source zone and its implications for the rupture nucleation, *J. Geophys. Res.*, *103*(B5), 9967–9986, doi:10.1029/97JB03670.

Zhao, D., H. Kanamori, H. Negishi, and D. Wiens (1996), Tomography of the source area of the 1995 Kobe earthquake: Evidence for fluids at the hypocenter?, *Science*, *274*, 1891–1894, doi:10.1126/science.274.5294.1891.

C. Chiarabba, L. Chiaraluce, M. Cocco, P. De Gori, R. Di Stefano, D. Piccinini, and L. Valoroso, Istituto Nazionale di Geofisica e Vulcanologia, Via di Vigna Murata, 605, I-00143 Rome, Italy. (raffaele.distefano@ingv.it)